Electronic Supporting Information

Preparation, characterization and electrocatalysis performance of a trimeric ruthenium-substituted isopolytungstate

Rong Wan, Huafeng Li, Xinyi Ma, Zhen Liu, Vikram Singh, Pengtao Ma, Chao Zhang, Jingyang Niu* and Jingping Wang*

Henan Key Laboratory of Polyoxometalate Chemistry, College of Chemistry and Chemical Engineering, Henan University, Kaifeng, Henan 475004, (P. R. China), Fax: (+86)-371-23886876, E-mail: jyniu@henu.edu.cn, jpwang@henu.edu.cn

Contents

Fig. S10 UV/Vis spectra of **1** in dilute solution at different pH values: (a) pH = 6.3–11.0; (b) pH = 2.5–6.3.

Fig. S11 IR spectra of compound **1** (black line) and before and precipitation obtained by addition of excess RbCl solids into 0.5 M NaCl solution (containing 1 mM **1**) after continuous cycling test 50 cycles (blue line).

Fig. S12 Negative ESI-MS spectra of the precipitate which obtained from treating electrolyte solution (containing the compound **1**).

Table S5 Electrocatalytic performance of nitrite oxidation for various catalysts or modified electrodes.

Fig. S13 TG curve of compound **1**.

Fig. S14 SEM image and EDX spectrum of single crystal of **1**.

Table S1. A summary of pure inorganic ruthenium-containing POMs with well-defined structures.

Compounds	Year	Ref.
$\{O[Ru^{IV}(X)P_2W_{17}O_{61}]_2\}^{16-}$ (X = OH, Cl)	1993	1
$[\{\alpha\text{-}SiW_{11}O_{39}Ru^{III}\}_2O]^{12-}$	2007	2
$[\{PW_{11}O_{39}\}_2\{(HO)Ru^{IV}\text{-}O\text{-}Ru^{IV}(OH)\}]^{10-}$	2008	3
$[\{Ru^{IV}_4O_4(OH)_2(H_2O)_4\}(\gamma\text{-}SiW_{10}O_{36})_2]^{10-}$	2008	4
$[Ru^{IV}_4Cl_4O_2(\mu\text{-}OH)_4(\gamma\text{-}SiW_{10}O_{36})_2]^{12-}$	2008	5
$[\gamma\text{-}XW_{10}O_{38}\{Ru^{IV}N\}_2]^{6-}$ (X = Si, Ge)	2009	6
$[(\gamma\text{-}PW_{10}O_{36})_2Ru^{IV}_4O_{5(}OH)(H_2O)_4]^{9-}$	2010	7
$[\{Ru^{IV}_4O_6(H_2O)_9\}_2Sb_2W_{20}O_{68}(OH)_2]^{4-}$	2012	8
$[\{Ru^{IV}_4O_6(H_2O)_9\}_2\{Fe(H_2O)_2\}_2\{\beta\text{-}TeW_9O_{33}\}_2H]^{4-}$	2012	8
$[H_2Mo^{VI}_{14}Ru^{IV}_2O_{50}(OH)_2]^{10-}$	2018	9
$[SeO_3(H_3Ru^{IV}W_{11}O_{38})_3]^{14-}$	2019	This work

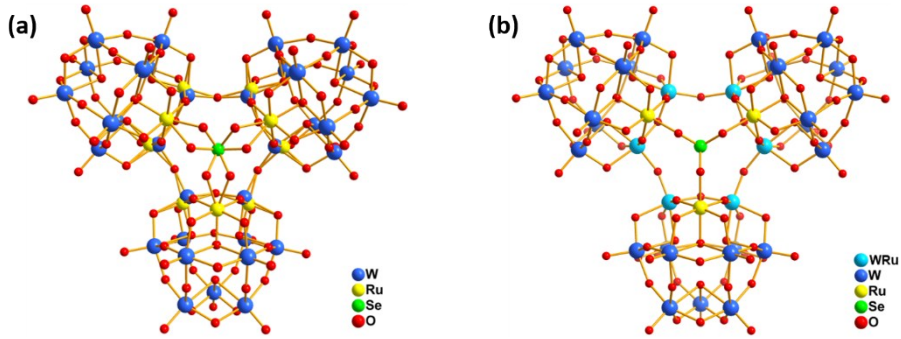

Fig. S1 (a) The actual polyoxoanion structure of **1** on the crystallography. (b) The simplified schematic of **1a**. O atoms around Se atom are disordered due to the symmetry, thus, we present **1a** with Fig. S1b briefly, so that we can be easily understand.

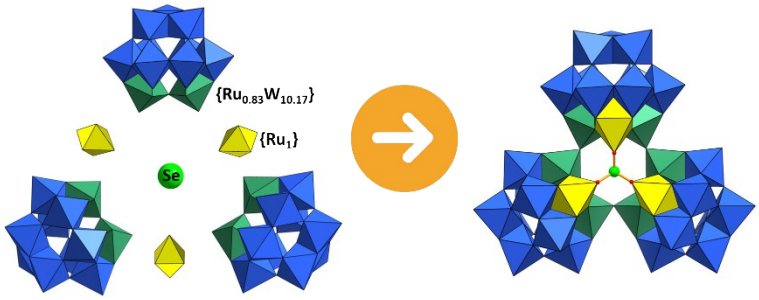

Fig. S2 Representation of the polyanion **1a** assembled from three building blocks $\{RuW_{11}\}$ in idealized C_{3v} symmetry. Colour code: WO_6 octahedra, blue; W/RuO_6 octahedra, sea green; RuO_6 octahedra, yellow; O, red balls; Se, green ball.

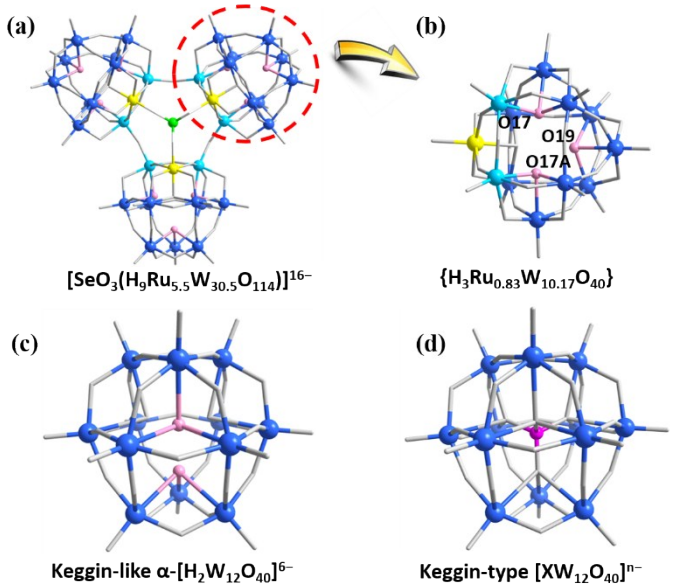

Fig. S3 Structures of polyanion **1a** (a) and $\{H_3Ru_{0.83}W_{10.17}O_{40}\}$ cluster (b) with BVS assignments; (c) Keggin-like iso-POT α-$\{H_2W_{12}O_{40}\}$ (metatungstate); (d) classical Keggin-type hetero-POT $[XW_{12}O_{40}]^{n-}$ (X = Si, P, Ge, As, et. al.) (W, blue balls; Se, green balls; Ru, yellow balls; monoprotonated O, pink balls; O^{2-} ligand, grey sticks, scheme outlined in Table S2).

Table S2. The BVS calculations of all crystallographically unique O atoms on **1a**.

Atom	BVS	Atom	BVS
O1	2.09	O13	1.96
O2	2.04	O14	1.96
O3	1.89	O15	2.07
O4	1.81	O16	2.00
O5	1.66	O17	0.80
O6	1.84	O18	1.85
O7	1.98	O19	1.18
O8	2.02	O20	1.66
O9	1.85	O21	1.89
O10	1.80	O22	1.85
O11	1.70	O23	1.80
O12	1.61	O24	1.74

Table S3. The BVS calculations of all crystallographically unique W, Se and Ru atoms on **1a**.

Atom lable	BVS	Atom lable	BVS
W1	6.14	W5	6.25
W2	6.01	W6	5.81
W3	6.06	Se1	3.84
W4	6.46	Ru1	4.07

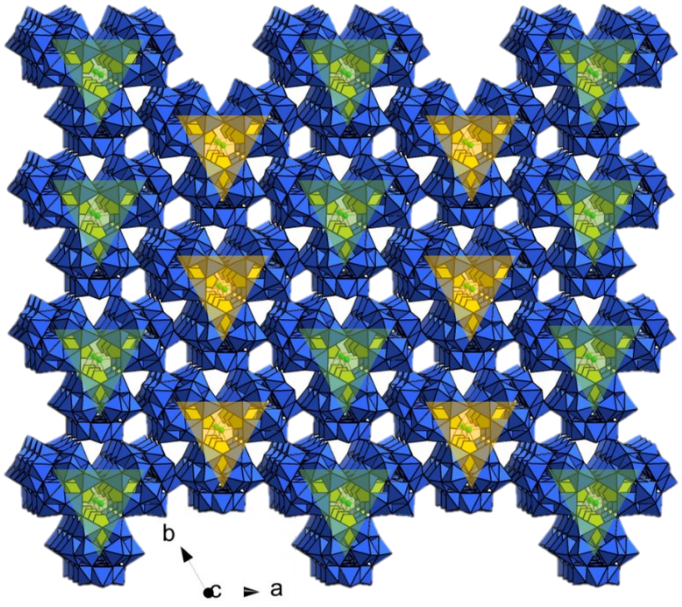

Fig. S4 The crystal packing arrangements of polyanions **1a** packing along the c axes and the simplified packing of **1a** viewed along the ab plane. Rb^{+}, Cl^{-} ions and lattice water molecules are neglected for the sake of clarity.

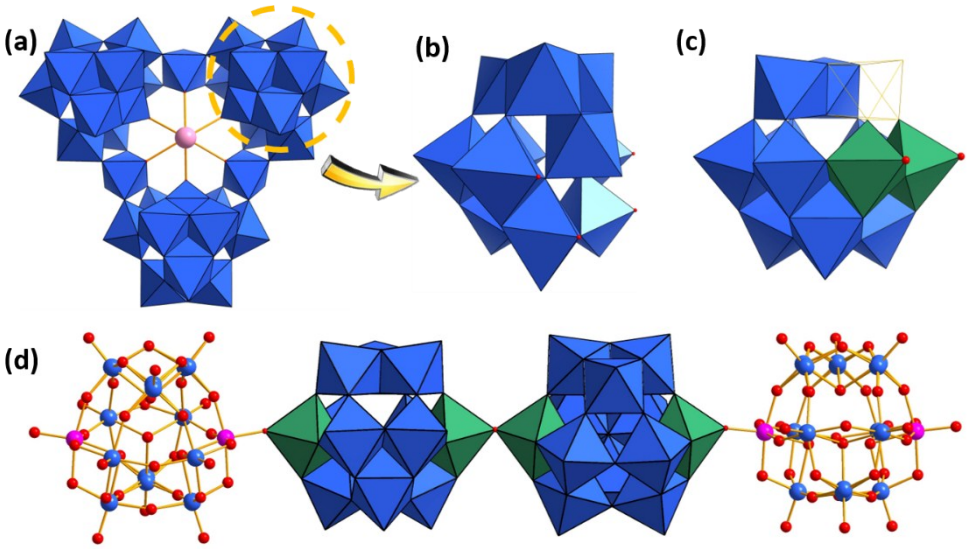

Fig. S5 (a) ball-and-stick representation of polyanion $\{(H_2O)_4K\subset[H_{12}W_{36}O_{120}]\}^{11-}$ ($\{W_{36}\}$); (b) the divacant $\{W_{11}\}$ building block in $\{W_{36}\}$ cluster; (c) the monovacant Keggin-like $\{H_3Ru_{0.83}W_{10.17}O_{40}\}$ building block in polyanion **1a**; (d) a chain-linked iso-POT $\{(DMAH)_6[H_4CoW_{11}O_{39}]\cdot 6H_2O\}_n$ based on monovacant Keggin-like $\{W_{11}\}$ subunit. Colour code: W/CoO_6 octahedra, sea green; W spheres, light blue; K sphere, rose; unordered W/Co spheres, pink.

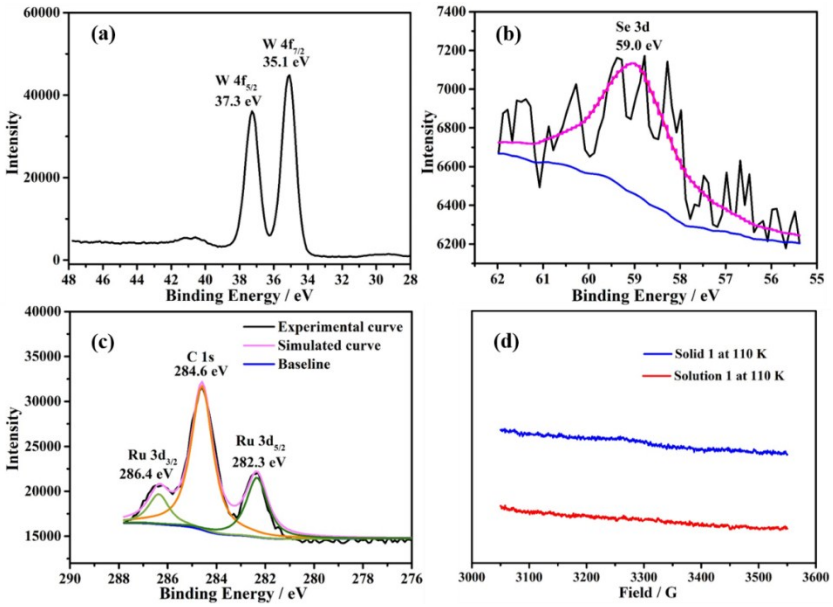

Fig. S6 XPS spectra for (a) W 4f, (b) Se 3d, and (c) Ru 3d. Spectra analysis was carried out using peak fitting with Gaussian–Lorentzian peak shape and Shirley type background subtraction, and the C 1s peak typically locates at 284.6 eV taking as a reference. (d) Low-temperature EPR spectra of compound **1**.

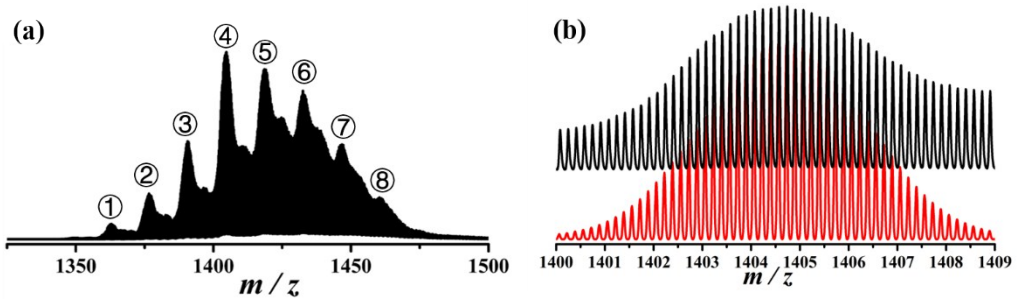

Fig. S7 (a) Negative ESI-MS spectrum of compound **1** in the selected range m/z = 1325–1500, and the detailed assignments were listed in Table S5; (b) Selected experimental (black) and simulated (red) mass spectra of the isotopic envelopes for at m/z = 1404.74 (–6). (Concentration, ca. 5×10^{-6} mol L^{-1}; Solvent, aqueous solution; Flow rate, 20 μL min^{-1})

Table S4. Detailed assignment of mass spectral data in the selected range m/z = 1325–1500.

Peak numbers	Formula	*m/z* (found)	*m/z* (calcd.)
1	$\{H_{10}[SeO_3(H_9Ru_{5.5}W_{30.5}O_{114})](H_2O)_2\}^{6-}$	1362.9109	1362.9520
2	$\{H_{10}[SeO_3(H_9Ru_{5.5}W_{30.5}O_{114})](H_2O)_7\}^{6-}$	1376.6036	1376.5293
3	$\{RbH_9[SeO_3(H_9Ru_{5.5}W_{30.5}O_{114})](H_2O)_7\}^{6-}$	1390.5895	1390.6059
4	$\{Rb_2H_8[SeO_3(H_9Ru_{5.5}W_{30.5}O_{114})](H_2O)_7\}^{6-}$	1404.7367	1404.6825
5	$\{Rb_3H_7[SeO_3(H_3RuW_{11}O_{38})_3](H_2O)_7\}^{6-}$	1418.5607	1418.7592
6	$\{Rb_4H_6[SeO_3(H_3RuW_{11}O_{38})_3](H_2O)_7\}^{6-}$	1432.7256	1432.8358
7	$\{Rb_5H_5[SeO_3(H_3RuW_{11}O_{38})_3](H_2O)_7\}^{6-}$	1446.8631	1446.9124
8	$\{Rb_6H_4[SeO_3(H_3RuW_{11}O_{38})_3](H_2O)_7\}^{6-}$	1460.8528	1460.9890

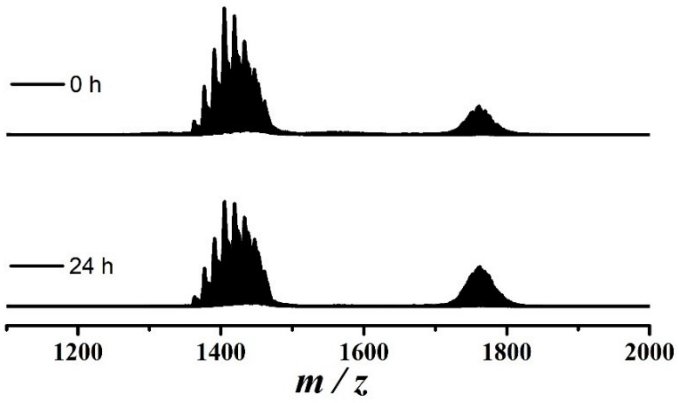

Fig. S8 Negative ESI-MS spectra of compound **1** in aqueous solution over 24 h.

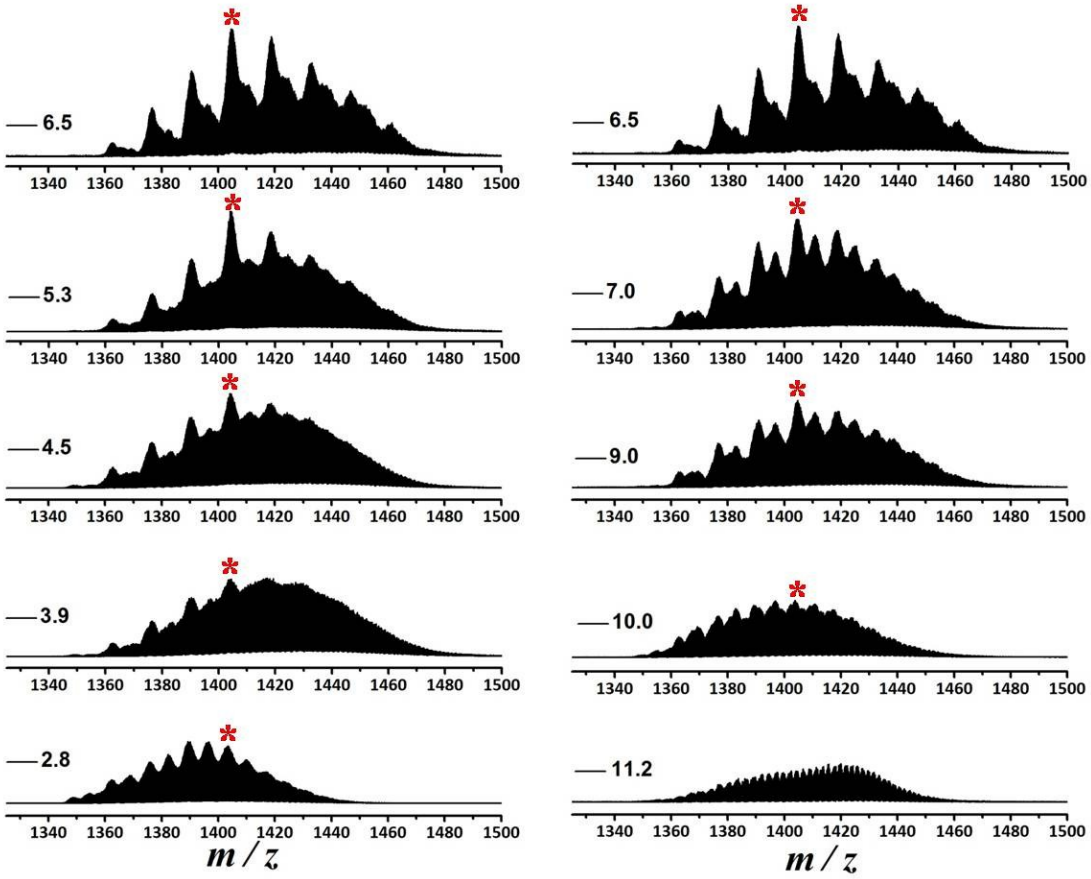

Fig. S9 Negative ESI-MS spectrum of compound **1** at different pH values in the selected range m/z = 1325–1500. Natural pH value reached 6.5 (±0.1) when compound **1** was dissolved into deionized water at about 5×10^{-6} mol L^{-1} concentration. Peaks with red asterisk (*) were all around 1404.7(−6), assigned to the species of the intact polyanion $\{Rb_2H_8[SeO_3(H_9Ru_{5.5}W_{30.5}O_{114})](H_2O)_7\}^{6-}$ (Concentration, ca. 5×10^{-6} mol L^{-1}; Solvent, aqueous solution; Flow rate, 20 μL min^{-1}).

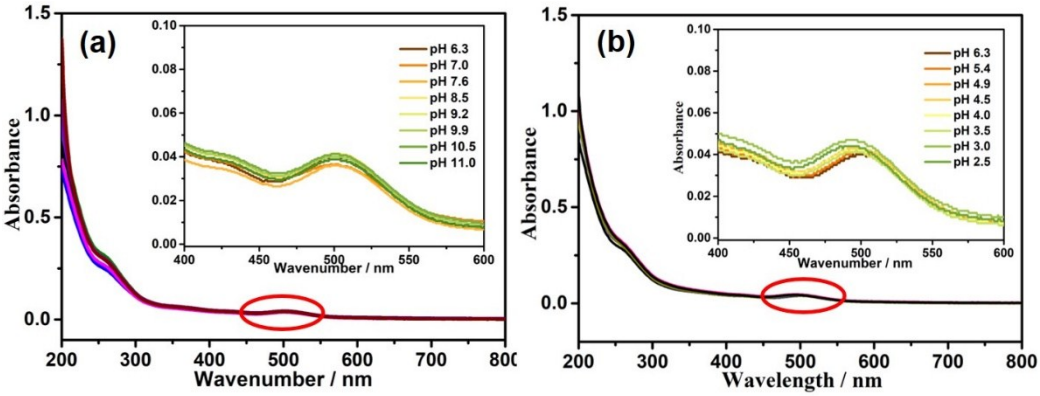

Fig. S10 UV/Vis spectra of **1** in dilute solution at different pH values: (a) pH = 6.3–11.0; (b) pH = 2.5–6.3.

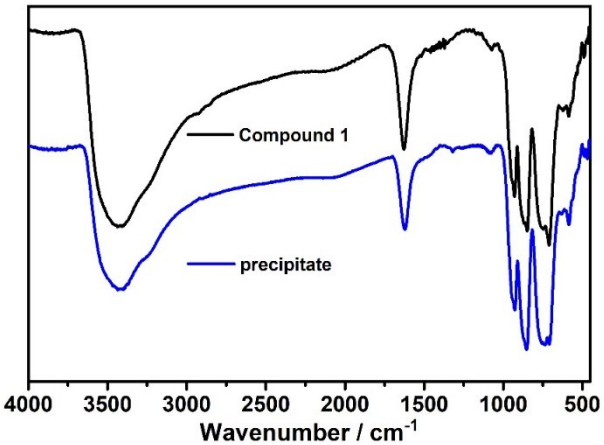

Fig. S11 IR spectra of compound **1** (black line) and before and precipitation obtained by addition of excess RbCl solids into 0.5 M NaCl solution (containing 1 mM **1**) after continuous cycling test 50 cycles (blue line).

IR spectra

The building block $\{H_3RuW_{11}O_{40}\}$ in compound **1** and metatungstate (namely saturated Keggin-like iso-POT α-$\{H_2W_{12}O_{40}\}$) is proved to share the similar structure, which has been described in crystallographic description. To undergird this result, IR spectra were recorded from two freshly prepared samples of compound **1** and $(n\text{-}Pr_4N)_4[H_4W_{12}O_{40}]$ obtained from Himeno,[14] both of which obviously exhibit three kinds of characteristic vibration derived from the Keggin-like framework in the wavenumber region of 1300–400 cm^{-1} (Fig. S11). For compound **1**, the vibrations of terminal $\nu(W–O_t)$ (pink region), edge-sharing $\nu(W–O_b)$ (yellow region) and corner-sharing $\nu(W–O_c)$ (blue region) vibrations can be figured out at 907 cm^{-1}, 846–823 cm^{-1} and 723–675 cm^{-1}, respectively, while in the case of $Na_6[H_2W_{12}O_{40}]$ they are located at 968 cm^{-1}, 918–884 cm^{-1} and 798 cm^{-1}. Obviously, three characteristic vibrations of compound **1**, by contrast, all show slightly red shifts than those of $Na_6[H_2W_{12}O_{40}]$, which may be concerned for the substitution of Ru decreasing the vibrational frequency of W–O bonds.[15]

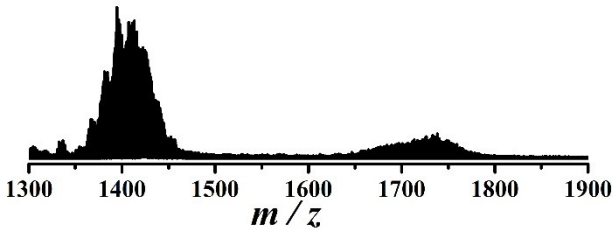

Fig. S12 Negative ESI-MS spectra of the precipitate which obtained from treating electrolyte solution (containing the compound **1**). (Solvent, aqueous solution; Flow rate, 20 μL min^{-1}). The Highest Peak m/z = 1395.46(−6) can be assigned to the species of the intact polyanion $\{Rb_2H_8[SeO_3(H_9Ru_{5.5}W_{30.5}O_{114})](H_2O)_4\}^{6-}$ (calcd. m/z = 1395.67(−6)).

Table S5. Electrocatalytic performance of nitrite oxidation for various catalysts or modified electrodes.

Catalysts/electrodes	electrolyte	Oxidation potential (E_0)	Peak Current (I_0)/ concentration of NO_2^-	Ref.
$PMo_{11}V$/PDDA-rGO	0.2 M PBS (pH 7.0)	≈ 0.84 V	≈ 47 μA / 0.5 mM	16
3D-mp-rGO–POM-GCE	0.1 M H_2SO_4	0.6–0.8 V (vs. SCE)	≈ 25 μA / 1 mM	17
Cu/MWCNTs-GC	0.1 M PBS (pH 7.0)	0.93 V (vs. SCE)	≈ 36 μA / 1 mM	18
Dend/AuNps(II)/Pt	0.1 mM $NaClO_4$	0.80 V (vs. SCE)	≈ 19 μA / 1 mM	19
Bare Pt	0.1 mM $NaClO_4$	0.88 V (vs. SCE)	≈ 13 μA / 1 mM	19
CU/MWCNT/Gr/GCE	0.1 M PBS (pH 7.0)	≈ 0.93 V (vs. SCE)	≈ 225 / 5 mM	20
GC/Ag–P(MMA-*co*-AMPS)	0.1 M PBS (pH 7.0)	0.80 V (vs. SCE)	≈ 33 μA / 1 mM	21
[VO(SB)]-CPE	0.1 M PBS (pH 4.0)	≈ 0.85 V (vs. SCE)	≈ 13 μA / 1 mM	22
AuNPs-S-Gr/GCE	0.1 M PBS (pH 4.0)	0.88 V (vs. Ag/AgCl)	≈ 132 μA / 4 mM	23
FeTMPyP/HTi_2NbO_7 NSs/GCE	0.2 M PBS (pH 7.0)	0.80 V (vs. SCE)	≈ 250 μA / 8 mM	24
Au NRs–Nafon-GCE	0.1 M PBS (pH 6.0)	≈ 0.83 V	≈ 19 μA / 0.5 mM	25
CR-GO/GCE	0.1 M PBS (pH 5.0)	0.82 V (vs. SCE)	≈ 68 μA / 1 mM	26
Catalyst **1** (bare GC)	0.5 M NaCl	0.83 V (vs. Ag/AgCl)	59 μA / 1 mM	here

Note: "GCE" and "GC" appeared in the first column are both referred to glassy carbon electrode, carbon paste electrode was cited as CPE.

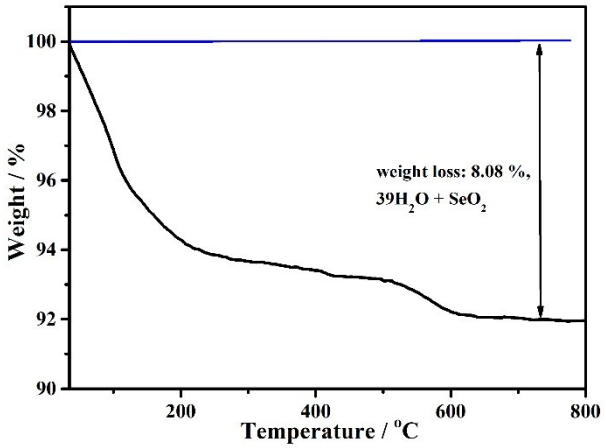

Fig. S13 TG curve of compound **1**. In the range of 35–800 °C, the black line shows one continuous mass loss, corresponding to the release of 39 lattice water molecules and the sublimation of SeO_2. The total fluid loss was a little lower than that of crystallographic analyses result owing to a small degree of crystal weathering.[27-29]

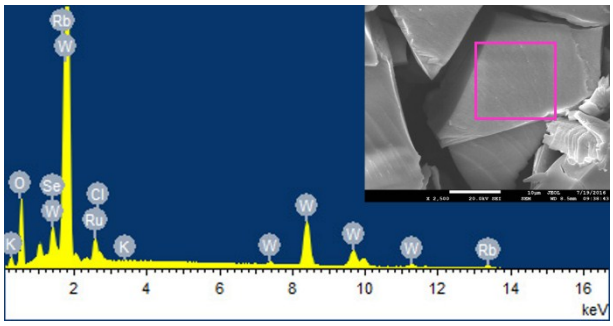

Fig. S14 SEM image and EDX spectrum of single crystal of **1**. Ru and W were detected with approximate ratio of 5.40: 1 (W: Ru).

References:

1 W. J. Randall, T. J. R. Weakley, R. G. Finke, *Inorg. Chem.*, 1993, **32**, 1068–1071.
2 M. Sadakane, D. Tsukuma, M. H. Dickman, B. S. Bassil, U. Kortz, M. Capron, W. Ueda, *Dalton Trans.*, 2007, 2833–2838.
3 S.-W. Chen, R. Villanneau, Y. Li, L.-M. Chamoreau, K. Boubekeur, R. Thouvenot, P. Gouzerh, A. Proust, *Eur. J. Inorg. Chem.*, 2008, 2137–2142.
4 (a) A. Sartorel, M. Carraro, G. Scorrano, R. D. Zorzi, S. Geremia, N. D. McDaniel, S. Bernhard, M. Bonchio, *J. Am. Chem. Soc.*, 2008, **130**, 5006–5007; (b) Y. Geletii, B. Botar, P. Kögerler, D. Hillesheim, D. Musaev, C. L. Hill, *Angew. Chem. Int. Ed.*, 2008, **47**, 3896–3899; (c) G. Süss-Fink, *Angew. Chem. Int. Ed.*, 2008, **47**, 5888–5890.
5 S. Yamaguchi, K. Uehara, K. Kamata, K. Yamaguchi, N. Mizuno, *Chem. Lett.*, 2008, **37**, 328–329.
6 C. Besson, D. G. Musaev, V. Lahootun, R. Cao, L.-M. Chamoreau, R. Villanneau, F. Villain, R. Thouvenot, Y. V. Geletii, C. L. Hill, A. Proust, *Chem. - Eur. J.*, 2009, **15**, 10233–10243.
7 C. Besson, Z. Huang, Y. V. Geletii, S. Lense, K. I. Hardcastle, D. G. Musaev, T. Lian, A. Proust, C. L. Hill, *Chem. Commun.*, 2010, **46**, 2784–2786.
8 I. V. Kalinina, N. V. Izarova, U. Kortz, *Inorg. Chem.*, 2012, **51**, 7442–7444.
9 R. Wan, Q. Xu, M. Han, P. Ma, C. Zhang, J. Niu, J. Wang, *Materials*, 2018, **11**, 178–190.
10 M. Han, Y. Niu, R. Wan, Q. Xu, J. Lu, P. Ma, C. Zhang, J. Niu, J. Wang, *Chem. Eur. J.,* 2018, **24**, 11059–11066.
11 S. Himeno, M. Yoshihara, M. Maekawa, *Inorg. Chim. Acta*, 2000, **298**, 165–171.
12 C. Boskovic, M. Sadek, R. T. C. Brownlee, A. M. Bond, A. G. Wedd, *J. Chem. Soc., Dalton Trans.*, 2001, 187–196.
13 C. R. Sprangers, J. K. Marmon, D. C. Duncan, *Inorg. Chem.*, 2006, **45**, 9628–9630.
14 S. Himeno, M. Yoshihara, M. Maekawa, *Inorg. Chim. Acta*, 2000, **298**, 165–171.
15 R. Wan, Y. Wang, M. Han, P. Ma, J. Niu, J. Wang, *Inorg. Chem. Commun.*, 2016, **68**, 72–75.
16 L. Zhang, S. Li, Z. Zhang, L. Tan, H. Pang, H. Ma, *J. Electroanal. Chem.*, 2017, **807**, 97–103.
17 G. Ma, M. Yang, F. Xu, L. Wang, *Anal. Methods*, 2017, **9**, 5140–5148.
18 D. Manoj, R. Saravanan, J. Santhanalakshmi, S. Agarwal, V. K. Gupta, R. Boukherrou, *Sens. Actuators B*

Chem., 2018, **266**, 873–882.
19 J. Losada, M. P. G. Armada, E. García, C. M. Casado, B. Alonso, *J. Electroanal. Chem.*, 2017, **788**, 14–22.
20 A. Abo-Hamad, M. A. AlSaadi, M. A. Hashim, *J. Electroanal. Chem.*, 2018, **812**, 107–114.
21 P. K. Rastogi, V. Ganesan, S. Krishnamoorthi, *J. Mater. Chem. A*, 2014, **2**, 933–943.
22 M. A. Kamyabi, F. Aghajanloo, *J. Electroanal. Chem.*, 2008, **614**, 157–165.
23 S. A. Bhat, S. A. Pandit, M. A. Rather, G. M. Rather, N. Rashid, P. P. Ingole, M. A. Bhat, *New J. Chem.*, 2017, **41**, 8347–8358.
24 M. Wang, Z. Fan, L. Yi, J. Xu, X. Zhang, Z. Tong, *J. Mater. Sci.*, 2018, **53**, 11403–11414.
25 D. Rao, J. Zhang, J. Zheng, *J. Iran. Chem. Soc.*, 2016, **13**, 2257–2266.
26 V. Mani, A. P. Periasamy, S.-M. Chen, *Electrochem. Commun.*, 2012, **17**, 75–78.
27 Y. Huo, Y.-C. Chen, S.-G. Wu, J.-H. Jia, W.-B. Chen, J.-L. Liu, M.-L. Tong, *Inorg. Chem.*, 2018, **57**, 6773−6777.
28 J. A. F. Gamelas, H. M. Carapuça, M. S. Balula, D. V. Evtuguin, W. Schlindwein, F. G. Figueiras, V. S. Amaral, A. M. V. Cavaleiro, *Polyhedron*, 2010, **29**, 3066–3073.
29 Z.-G. Lin, B. Wang, J. Cao, B.-K. Chen, Y.-Z. Gao, Y.-N. Chi, C. Xu, X.-Q. Huang, R.-D. Han, S.-Y. Su, C.-W. Hu, *Inorg. Chem.*, 2012, **51**, 4435−4437.